Research Square

Preprints are preliminary reports that have not undergone peer review.
They should not be considered conclusive, used to inform clinical practice,
or referenced by the media as validated information.

Temporal changes in root carbon and nitrogen partitioning and trehalose-associated freezing protection in Medicago ruthenica

Jing Xing
Inner Mongolia Agricultural University
Yingtong Mu
University of Science and Technology of China
Jiani Wang
Ulanqab City Academy of Agricultural and Forestry Sciences, Chahar Right Front Banner
Kefan Cao
Inner Mongolia Agricultural University
Wenqiang Fan
Inner Mongolia Agricultural University
Yutong zhang
Inner Mongolia Agricultural University
Fengling Shi
shifengling@imau.edu.cn

Inner Mongolia Agricultural University

Research Article

Keywords: Medicago ruthenica, freezing stress, root physiology, carbon–nitrogen partitioning, trehalose

Posted Date: November 25th, 2026

DOI: https://doi.org/10.21203/rs.3.rs-11606094/v1

License: This work is licensed under a Creative Commons Attribution 4.0 International License.
Read Full License

Additional Declarations: No competing interests reported.

Temporal changes in root carbon and nitrogen partitioning and trehalose-associated freezing protection in *Medicago ruthenica*

Jing Xing [a]，Yingtong Mu [b]，Jiani Wang [c]，Kefan Cao [a], Wenqiang Fan [a]，Yutong zhang [a]，Fengling Shi [a*]

[a] Key Laboratory of Grassland Resources of the Ministry of Education, College of Grassland Science, Inner Mongolia Agricultural University, Hohhot 010010, China

[b] School of Life Sciences, USTC Life Sciences and Medicine, University of Science and Technology of China, Hefei, 230000, China

[c] Ulanqab City Academy of Agricultural and Forestry Sciences, Chahar Right Front Banner, Ulanqab, 012000, China

Corresponding author: Fengling Shi

E-mail: shifengling@imau.edu.cn

Abstract

Background: Root survival and recovery during freezing are associated with changes in carbon and nitrogen metabolism, but the relationships between resource partitioning and protective carbohydrates remain poorly resolved in perennial forage legumes. We investigated temporal root responses in *Medicago ruthenica* and tested the effects of pharmacological manipulation of trehalose metabolism.

Results: Plants were exposed to −10 °C for 2, 7, or 14 d, with post-freezing performance assessed after 7 d of recovery. Physiological measurements, dual $^{13}C/^{15}N$ tracing, transcriptomics, metabolomics, and multiblock integration distinguished a 7-d state with stronger nitrogen- and amino-acid-associated responses and greater injury from a 14-d state with greater starch depletion, soluble-sugar accumulation, and lower injury. The freezing-induced increase in the root share of recovered ^{15}N was approximately 15 percentage points at 7 d and 3 at 14 d, whereas the corresponding changes for ^{13}C were approximately −4 and +8 percentage points. Starch–sucrose turnover and trehalose–galactinol–raffinose metabolism were prominent in the 14-d molecular profile. Exogenous trehalose reduced electrolyte leakage and malondialdehyde accumulation, maintained root metabolic activity, and improved survival and regrowth. The tested equimolar mannitol, sorbitol, and sucrose treatments generally produced weaker effects. Validamycin A reduced

trehalase activity and increased trehalose content; combined validamycin A and trehalose treatment produced among the strongest protective responses.

Conclusions: Distinct root metabolic states at 7 and 14 d were associated with different relative carbon and nitrogen tracer partitioning. Trehalose supplementation, alone or combined with trehalase inhibition, provides an effective strategy for protecting roots during freezing and improving post-freezing recovery in *M. ruthenica*.

Keywords: *Medicago ruthenica*; freezing stress; root physiology; carbon–nitrogen partitioning; trehalose;

Background

Freezing episodes limit establishment, overwintering, and spring regrowth of perennial forage legumes by causing extracellular ice formation, cellular dehydration, membrane destabilization, and oxidative injury [1,2]. Although leaves provide conspicuous injury symptoms, root integrity is critical for water and nutrient acquisition and can strongly influence post-thaw recovery. *Medicago ruthenica*, a wild perennial legume closely related to alfalfa, is distinguished by broad environmental stress tolerance and is an important genetic resource for forage improvement [3]. Cold-related research in Medicago has identified links among cold-regulated transcription factors, cryoprotective sugars, antioxidant defenses, and post-freezing survival [4,5]. However, the relationship between temporal changes in root resource partitioning and the function of candidate protective metabolites remains insufficiently resolved in *M. ruthenica*.

Plant responses to freezing are strongly time dependent, and different phases of stress may differentially involve nitrogen metabolism, carbon allocation, compatible-solute accumulation, and cellular protection. A recent genetic study in Arabidopsis connected root freezing tolerance with a NAC056–CBF–NIA1 module that coordinates CBF signaling, nitrate assimilation, and root growth [6], illustrating that nitrogen economy is part of the freezing response rather than a passive consequence of growth inhibition. Carbon and nitrogen, however, are usually measured as static concentrations, so changes in pool size can be confused with altered import, turnover, or dilution. Dual $^{13}C/^{15}N$ tracing with time-matched controls can resolve differences in the relative partitioning of recovered carbon and nitrogen tracers among organs. This approach is particularly relevant for roots, where carbon supply from source tissues and local nitrogen assimilation must remain coordinated during extended stress.

Carbohydrate metabolism is a plausible biochemical bridge between altered allocation and freezing protection. Mobilization of starch and adjustment of sucrose turnover can increase soluble carbon available for osmotic balance, membrane stabilization, redox buffering, and recovery. Within this network, trehalose-6-phosphate (T6P) and trehalose are especially interesting because they couple sucrose status with growth and stress metabolism [7]. Overexpression of *OsTPS1* improved cold tolerance in rice [8], and the SAPK10–ABF1–TPS2 pathway increased endogenous trehalose and chilling tolerance, with exogenous trehalose rescuing a sensitive mutant [9]. Overexpression and silencing of the class II TPS gene *VaTPS9* have further linked this gene to cold tolerance and reactive oxygen species homeostasis [10]. Raffinose-family oligosaccharides may operate alongside trehalose: cold-inducible galactinol synthase increased galactinol, raffinose, and chilling tolerance in transgenic rice [11], whereas raffinose manipulation did not universally alter Arabidopsis freezing tolerance [12]. In contrast, suppression of raffinose breakdown increased endogenous raffinose and freezing tolerance in petunia [13]. These apparently divergent outcomes argue against treating any single sugar as a universal determinant and instead support testing a context-dependent trehalose–sucrose–galactinol–raffinose module.

Three questions motivate this study. First, how do root injury, metabolism, and post-freezing performance differ with exposure duration? Second, how are changes in relative root carbon and nitrogen tracer partitioning associated with transcriptomic and metabolomic responses? Third, does pharmacological manipulation of a carbohydrate pathway prioritized by these profiles alter freezing-related injury and recovery? Validamycin A increased trehalose in *Medicago truncatula* root nodules without a corresponding increase in ordinary roots or leaves [14], emphasizing the need to measure trehalase activity and trehalose in the tissue being tested. Trehalose supplementation, equimolar sugar and polyol controls, and trehalase inhibition provide complementary tests of the contribution of trehalose to root freezing tolerance.

Here, we combined physiological and injury measurements with dual $^{13}C/^{15}N$ tracing, root transcriptomics, metabolomics, targeted metabolite quantification, and multiblock integration to examine *M. ruthenica* exposed to −10 °C for 2, 7, or 14 d. We then evaluated exogenous trehalose and validamycin A, together with sugar and polyol controls and short-term expression measurements. This design integrates temporal analyses of root carbon and nitrogen metabolism with pharmacological tests of the protective role of trehalose during freezing.

Methods

Plant material and freezing treatment

Seeds of *Medicago ruthenica* (L.) Trautv. cv. 'Zhilixing' were mechanically scarified, germinated, and transferred individually to 32-cell trays containing vermiculite. Plants were supplied regularly with Hoagland nutrient solution and maintained at 25 °C under a 16-h light/8-h dark photoperiod and 50% relative humidity. Uniform plants at the branching stage, approximately 30 cm in height, were randomly assigned to experimental treatments.

For the freezing experiment, control plants were maintained at 25 °C and treated plants were exposed to −10 °C. Roots were sampled after 2, 7, and 14 d. The physiological time course included recovery for 7 d at 25 °C after the 14-d treatment (F14d + R7d). Exposure-duration comparisons of survival and regrowth were assessed after 7 d of recovery following freezing for 2, 7, or 14 d, as shown in Fig. 2. Time-matched controls were maintained at 25 °C for the corresponding duration. Fresh tissues were used for physiological measurements or frozen in liquid nitrogen and stored at −80 °C for molecular analyses.

Freezing injury and physiological measurements

Root soluble sugars were quantified using an anthrone colorimetric assay kit (KTB1320, Abbkine, Wuhan, China), starch by acid hydrolysis followed by anthrone colorimetry, free amino acids by ninhydrin colorimetry, and MDA using a thiobarbituric acid assay kit (A003-2-2, Nanjing Jiancheng Bioengineering Institute, Nanjing, China). Sucrose synthase activity in the cleavage direction (SS-I), glutamine synthetase (GS), superoxide dismutase (SOD), and peroxidase (POD) were assayed using KTB3140, KTB3042, KTB1030, and KTB1150 kits, respectively (Abbkine). Enzyme activities are expressed as U g^{-1} FW, with units defined by the corresponding assay protocol. Fresh-weight normalization expresses activity per unit tissue mass. Soluble protein was determined by the Bradford method. The specified SOD assay measures inhibition of a xanthine oxidase-coupled reaction at 450 nm, whereas the specified POD assay monitors a peroxidase-dependent color reaction at 460 nm. Total C and N were measured in dried, ground roots using an elemental analyzer (Vario EL cube, Elementar). The elemental C/N ratio was calculated on a mass basis.

Electrolyte leakage was calculated as EL (%) = $C_1/C_2 \times 100$, where C_1 represents conductivity after incubation in deionized water at 25 °C for 2 h and C_2 represents total conductivity after boiling in a water bath for 20 min. Root metabolic activity was determined by TTC reduction using 0.5 g fresh tissue incubated

for 12 h at 37 °C, and TPF formation was quantified against a standard curve and expressed as mg TPF g^{-1} FW h^{-1}. Evans blue uptake was quantified at 600 nm after staining, removal of excess dye by washing, and extraction with formamide. Maximum photochemical efficiency of PSII (Fv/Fm) was determined after dark adaptation. Freezing tolerance was further characterized using challenge temperatures of 0, −5, −10, −15, and −20 °C, and the temperature producing 50% electrolyte leakage (EL50) was estimated by nonlinear sigmoidal regression. Following 7 d of recovery, survival was calculated as the number of surviving plants divided by the number of plants originally assigned to each freezing treatment × 100.

Dual-isotope labeling and relative organ partitioning

Both control and freezing-treatment plants were labeled once with each isotope tracer before the onset of freezing. Uniform plants received a single application of $^{15}NH_4Cl$ (10 atom% ^{15}N; 2 mmol L^{-1}; 10 mL $plant^{-1}$) 24 h before freezing. A single 4-h $^{13}CO_2$ pulse, generated from 1.2 g $Ba^{13}CO_3$ (99 atom% ^{13}C), was administered before freezing in a sealed chamber at 25 °C under a photosynthetic photon flux density of 400 μmol m^{-2} s^{-1}. Following this pre-treatment labeling, tracer distribution was assessed at harvest on days 7 and 14 after treatment initiation. Root samples collected from the control and freezing groups at 7 d were designated MC2 and ML2, respectively, and the corresponding samples collected at 14 d were designated MC3 and ML3, with three biological replicates per group. Roots were rinsed repeatedly with deionized water to remove externally adsorbed label. Plants were separated into roots, stems, and leaves, dried, ground, and analyzed for total C, total N, $\delta^{13}C$, and $\delta^{15}N$. Natural-abundance-corrected tracer recovery was calculated from organ biomass, elemental concentration, and isotope atom-fraction excess. The allocation to an organ was its recovered tracer pool divided by the sum of the recovered pools in all three organs, multiplied by 100. Treatment-induced changes in root allocation were calculated as freezing minus the time-matched control and expressed in percentage points.

Transcriptomic and metabolomic analyses

Total RNA was extracted using TRIzol reagent (Invitrogen), and RNA integrity was assessed using an Agilent 2100 Bioanalyzer, with samples meeting a RIN threshold of 6.5. Libraries were prepared using NEBNext® Ultra™ RNA Library Prep Kit for Illumina and sequenced on an Illumina NovaSeq 6000 using paired-end 150-bp sequencing. Raw reads were quality-filtered, rRNA sequences were removed, and clean reads were aligned to the *M. ruthenica* reference genome. Differentially expressed genes were identified

using DESeq2 with FDR < 0.05 and $|\log_2$ fold change$| > 1$, followed by GO and KEGG enrichment analyses. Selected genes representing nitrogen/amino-acid metabolism, starch/sucrose turnover, trehalose/RFO metabolism, and cold/redox protection were validated by qRT-PCR.

The same treatment groups were analyzed by UPLC–MS/MS metabolomic profiling. PCA and differential-metabolite analyses used normalized metabolite abundances, followed by KEGG pathway enrichment. Authentic standards were used for targeted quantification of D-trehalose, trehalose-6-phosphate, D-sucrose, galactinol, raffinose, L-proline, and trans-4-hydroxy-L-proline. Trehalose and the other compounds in Fig. 5E are expressed as mg g^{-1} FW; T6P in Fig. 7A is expressed as nmol g^{-1} FW. Targeted concentrations refer to tissue fresh weight and are distinct from the standardized abundance scores used in heatmaps.

qRT-PCR validation comprised six biological replicates, each measured in three technical replicates. Technical replicates were summarized within each biological sample before statistical comparison. Pharmacological expression profiles were measured at 0, 6, and 24 h. Heatmap values are presented as $\log_2$ relative expression, for which $\log_2(2^{-}\Delta\Delta Cq) = -\Delta\Delta Cq$. Negative values therefore represent expression below the calibrator on the logarithmic scale, rather than negative transcript abundance. The transcriptome-validation plot compares $\log_2$ fold changes from qRT-PCR and RNA-seq.

Multiblock data integration

Physiological, isotope, transcriptomic, and metabolomic datasets were integrated at the level of matched biological replicates using the R package multiblock (v0.8.11). Each sample identifier represented the same experimental unit across the four data blocks. Positive abundance variables were $\log_2$-transformed before Pareto scaling. Signed isotope values and allocation changes were centered and scaled without direct logarithmic transformation. Multiblock ordination was used to describe joint variation among groups, and feature stability was summarized by selection frequency across 1,000 balanced resamples using the fixed random seed 12345. Selection frequency was calculated as the number of resamples retaining a variable divided by 1,000. Ordination and resampling were interpreted as exploratory summaries of this dataset rather than independent predictive validation.

Only the three biological replicates per treatment × time group with complete matched measurements across all four blocks were included in integration (12 samples in total); the remaining physiological/isotope replicates were used only for univariate analyses.

Pairwise RV coefficients summarized cross-block similarity. Cross-omics network edges were retained at $|r| \geq 0.6$ and Benjamini–Hochberg-adjusted $P < 0.01$ using Pearson correlations. Module–trait associations were also calculated using Pearson correlations with multiple-testing correction. These associations were interpreted as exploratory because all blocks shared treatment and time effects.

Pharmacological treatments and short-term expression responses

Trehalose, mannitol, sorbitol, and sucrose were applied at 10 mmol L^{-1} by root drench for 24 h before freezing; validamycin A was applied at 50 μmol L^{-1} over the same pretreatment interval. The eight groups were Control, Freezing, F + Tre, F + Man, F + Sor, F + Suc, F + VA (validamycin A), and F + VA + Tre. Equivalent solvent controls were included where applicable. Root endpoints comprised trehalose (mg g^{-1} FW), T6P (nmol g^{-1} FW), trehalase activity (U g^{-1} FW), electrolyte leakage (%), MDA (nmol g^{-1} FW), TTC reduction (mg TPF g^{-1} FW h^{-1}), and SOD and POD activities (U g^{-1} FW). Survival (%) and shoot and root regrowth biomass (g $plant^{-1}$) characterized recovery. Each endpoint had six biological replicates per treatment. The four groups Freezing, F + Tre, F + VA, and F + VA + Tre were compared for expression of *MrTPS1*, *MrTPP1*, *MrTRE1*, *MrSUS6*, *MrAMY3*, *MrGOLS1*, *MrCBF3*, *MrCOR47*, and *MrAPX2* at 0, 6, and 24 h.

Statistical analysis

The biological replicate was the experimental unit. Data are presented as means ± SE. Physiological time courses were assessed using fixed effects of treatment, sampling time, and their interaction, with multiplicity-adjusted comparisons between freezing and control conditions at each time. Single-endpoint pharmacological traits were compared across the eight treatment groups; time was not included as a factor for panels 7A–E. Survival was treated as a binomial outcome using surviving and total plant counts. Expression profiles comprised four treatments and three sampling times, with technical replicates nested within biological samples and summarized before inference. The four-group trehalose/validamycin comparison was interpreted as evidence of combined-treatment responses, without inferring synergy from the rank of group means. Challenge-temperature electrolyte-leakage responses were characterized by nonlinear logistic regression. Within-time isotope and targeted-metabolite comparisons used two-sided t-tests as specified in the figure legends. Omics enrichment and cross-omics correlations were corrected using

the Benjamini–Hochberg procedure. Statistical significance was defined at $P < 0.05$ unless a stricter threshold is specified.

Results

Freezing elicits time-dependent changes in root carbon and nitrogen metabolism

Root carbon- and nitrogen-related traits in *Medicago ruthenica* varied with freezing duration and recovery (Fig. 1B–H). Root soluble sugar content increased significantly after freezing and continued to rise with treatment duration, reaching its maximum at 14 d before partially declining during recovery (Fig. 1B). By contrast, starch content progressively decreased under freezing and reached its minimum at 14 d, followed by substantial restoration after recovery (Fig. 1C). Consistent with altered carbohydrate metabolism, sucrose synthase activity increased during freezing and peaked at 14 d (Fig. 1D). The elemental C/N ratio showed little change at 2 d but increased significantly at 7 d and reached its highest value at 14 d, indicating a progressive increase in the root C/N ratio during prolonged freezing (Fig. 1E). Nitrogen-related traits displayed a different temporal pattern: free amino acid content and glutamine synthetase activity increased rapidly and both reached their highest levels at 7 d before declining at 14 d and during recovery (Fig. 1F, G). Meanwhile, MDA accumulation increased sharply during the early phase of freezing, peaked at 7 d, and subsequently declined despite continued stress exposure (Fig. 1H). Together, the measured traits revealed distinct temporal patterns, with stronger nitrogen/amino-acid-associated responses and injury at 7 d and more pronounced carbohydrate mobilization with lower injury at 14 d. We therefore next examined whether this metabolic transition was accompanied by corresponding changes in freezing injury, root activity and post-stress recovery capacity.

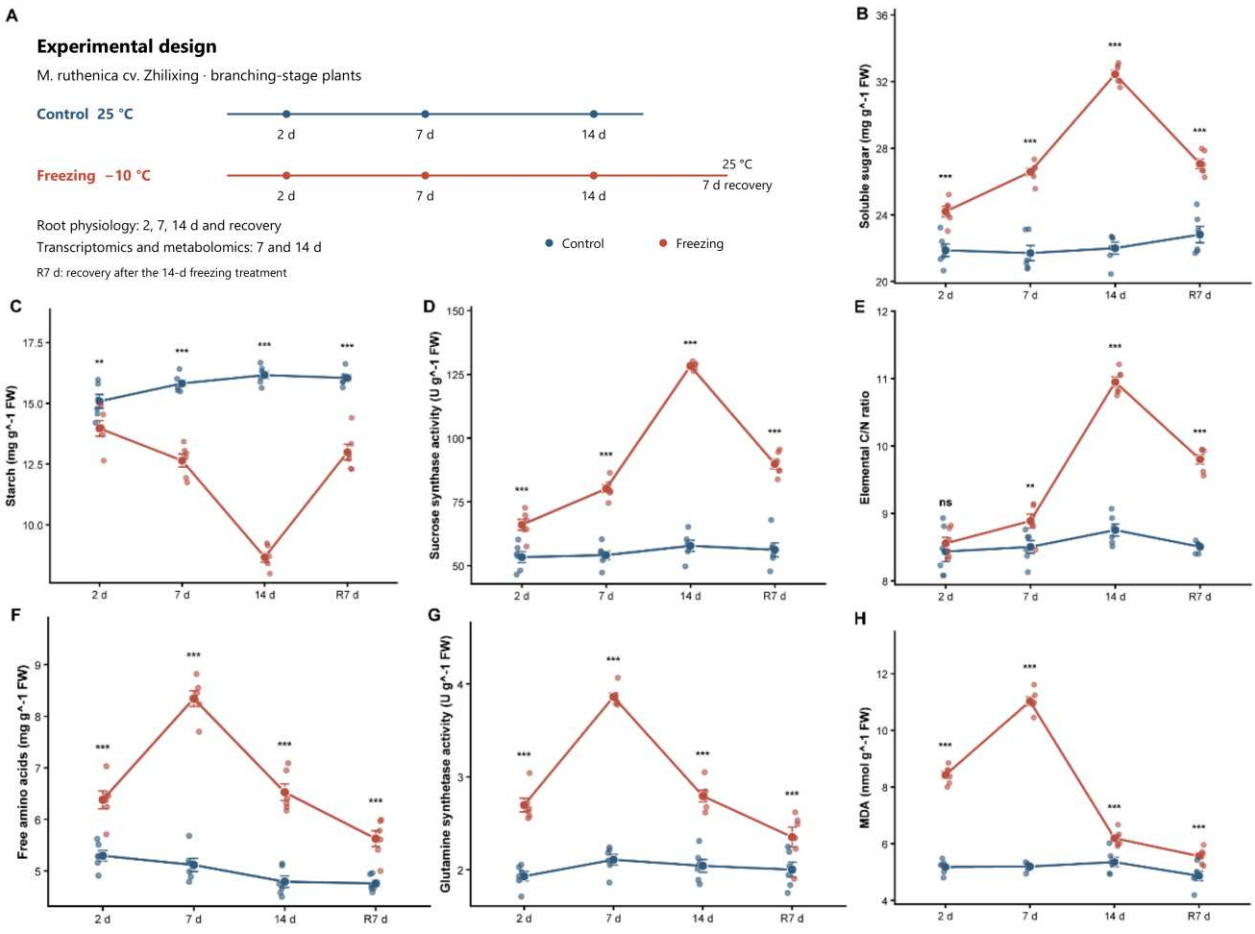

Fig. 1. Root carbon–nitrogen metabolism and membrane lipid peroxidation during freezing and recovery.

(A) Experimental design showing the control and freezing conditions, physiological sampling points, omics sampling stages, and recovery interval. Blue and red indicate control and freezing treatments, respectively. (B) Root soluble sugar content measured after 2, 7 and 14 d of freezing treatment and after 7 d of recovery. (C) Root starch content measured at the corresponding freezing and recovery time points. (D) Root sucrose synthase activity in the cleavage direction measured during freezing treatment and recovery. (E) Elemental C/N ratio of roots during freezing treatment and recovery. (F) Root free amino acid content during freezing treatment and recovery. (G) Root glutamine synthetase activity during freezing treatment and recovery. (H) Root malondialdehyde content during freezing treatment and recovery. For panels B–H, roots were collected from control and freezing-treated plants at 2, 7 and 14 d and after 7 d of recovery. n = 6 independent biological replicates per treatment × time point. Points and error bars represent means ± SE; individual points, where shown, represent biological replicates. Data were analyzed using two-way ANOVA with treatment, time, and their interaction. Asterisks indicate significant differences between control and freezing treatments at the corresponding time point: *P < 0.05, **P < 0.01, and ***P < 0.001; ns, not significant. C/N, carbon-to-nitrogen ratio; SS, sucrose synthase; GS, glutamine synthetase; MDA, malondialdehyde; FW, fresh weight; R7 d, 7 d of recovery.

Root injury and post-freezing recovery differ among exposure durations

Freezing injury and post-freezing performance differed among exposure durations (Fig. 2). Root electrolyte leakage was highest in the 7-d group and lower in the 14-d and recovery samples (Fig. 2A). After 7 d of recovery, plants previously exposed to freezing for 7 d showed the lowest survival, whereas

the 14-d exposure group showed higher survival (Fig. 2B). Shoot and root dry biomass after recovery followed a similar pattern, with lower values after 7-d than after 14-d freezing (Fig. 2C). Root TTC activity was lowest in the 7-d group and higher in the 14-d and recovery samples (Fig. 2D). Challenge-temperature assays showed different electrolyte-leakage response curves among the pretreatment groups (Fig. 2E). After recovery, Evans blue uptake was highest and Fv/Fm lowest in plants previously exposed for 7 d; both indicators showed less impairment in the 14-d exposure group (Fig. 2F). Thus, the 14-d group showed lower measured injury and better subsequent recovery performance than the 7-d group. We next examined the relative partitioning of recovered carbon and nitrogen tracers in relation to these response states.

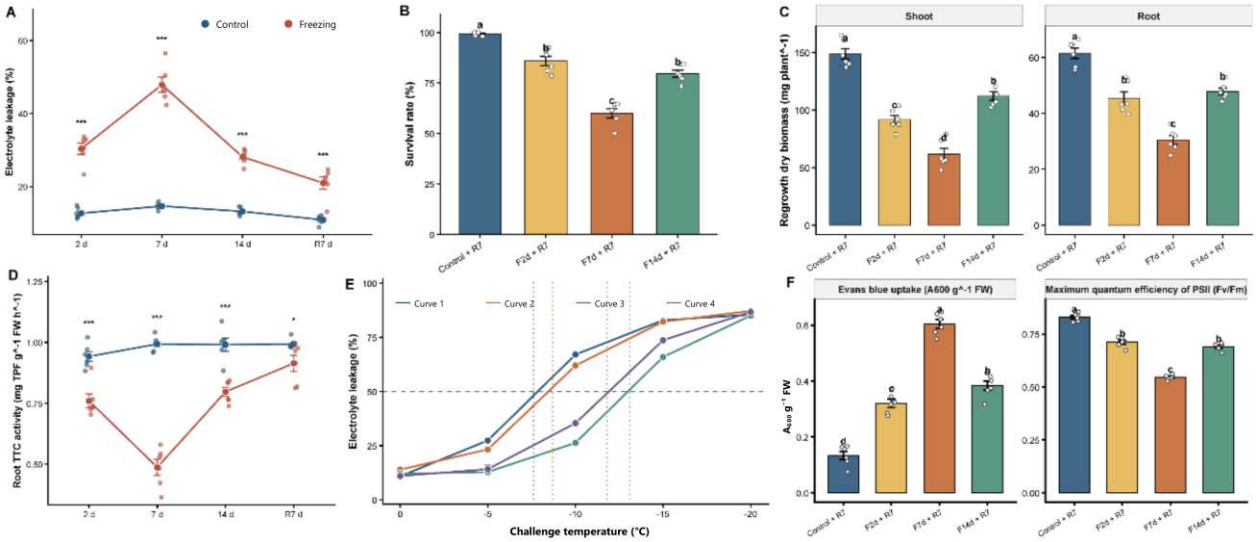

Fig. 2. Root injury, freezing sensitivity, and post-freezing recovery.

(A) Electrolyte leakage of roots measured after 2, 7 and 14 d of freezing treatment and after 7 d of recovery. (B) Survival rate determined after 7 d of recovery following control treatment or freezing exposure for 2, 7 or 14 d. (C) Shoot and root dry biomass measured after the 7-d recovery period following control treatment or freezing exposure for 2, 7 or 14 d. (D) Root TTC activity measured after 2, 7 and 14 d of freezing treatment and after 7 d of recovery. (E) Electrolyte leakage measured after exposure to a series of challenge temperatures (0, −5, −10, −15 and −20 °C). Curve identifiers distinguish the four displayed temperature-response series; dashed lines denote the 50% leakage level and the corresponding curve-specific temperature estimates. (F) Evans blue uptake and maximum quantum efficiency of photosystem II (Fv/Fm) measured after recovery from control treatment or freezing exposure for 2, 7 or 14 d. For panels A–F, n = 6 independent biological replicates per treatment. Survival rate data were analyzed as binomial responses. Shoot and root biomass and Evans blue uptake were measured after the 7-d recovery period. Root TTC measurements are shown for the sampling points indicated in panel D. Root viability was quantified using the TTC reduction assay and expressed as mg TPF g^{-1} FW h^{-1}. Evans blue uptake was quantified spectrophotometrically at 600 nm and normalized to fresh weight. Challenge-temperature curves summarize electrolyte-leakage responses and the corresponding 50% leakage thresholds. Bars represent means ± SE. Different lowercase letters indicate significant differences among treatments at $P < 0.05$; asterisks indicate significant pairwise differences where shown. EL, electrolyte leakage; TTC, triphenyl

tetrazolium chloride; TPF, triphenyl formazan; Fv/Fm, maximum quantum efficiency of PSII; FW, fresh weight.

Relative carbon and nitrogen tracer partitioning differs between sampling stages

Stable-isotope tracing revealed contrasting temporal patterns of carbon and nitrogen tracer partitioning to roots at 7 and 14 d (Fig. 3). Root $\delta^{15}N$ was higher under freezing at both 7 and 14 d. Organ-level allocation analysis showed that the freezing-induced increase in the root share of recovered ^{15}N tracer was substantially greater at 7 d than at 14 d (Fig. 3A, C). In contrast, root $\delta^{13}C$ showed no significant freezing-induced increase at 7 d but increased markedly at 14 d. Consistently, organ-level partitioning showed a higher root share of recovered ^{13}C tracer at 14 d under freezing (Fig. 3B, D). Organ-level partitioning further resolved these contrasting temporal responses. At 7 d, the proportion of ^{15}N allocated to roots increased from approximately 32% in the control to 47% under freezing, whereas at 14 d the corresponding increase was much smaller, from approximately 34% to 37% (Fig. 3C). Conversely, root ^{13}C allocation decreased from approximately 24% to 20% at 7 d but increased from approximately 26% to 34% at 14 d (Fig. 3D). Expressed as treatment-induced changes, freezing therefore caused an approximately +15-percentage-point increase in root ^{15}N allocation but a −4-percentage-point change in root ^{13}C allocation at 7 d, whereas at 14 d the response shifted to approximately +3 percentage points for ^{15}N and +8 percentage points for ^{13}C (Fig. 3E). Plotting these allocation changes together clearly separated the two stages, with the 7-d response occupying an N-biased allocation space and the 14-d response shifting toward a C-biased state (Fig. 3F). These isotope data provide direct evidence that the relative partitioning of recovered ^{13}C and ^{15}N tracers to roots differed between the 7- and 14-d sampling stages. We next examined whether these differences in relative tracer partitioning were accompanied by differences in transcriptional responses.

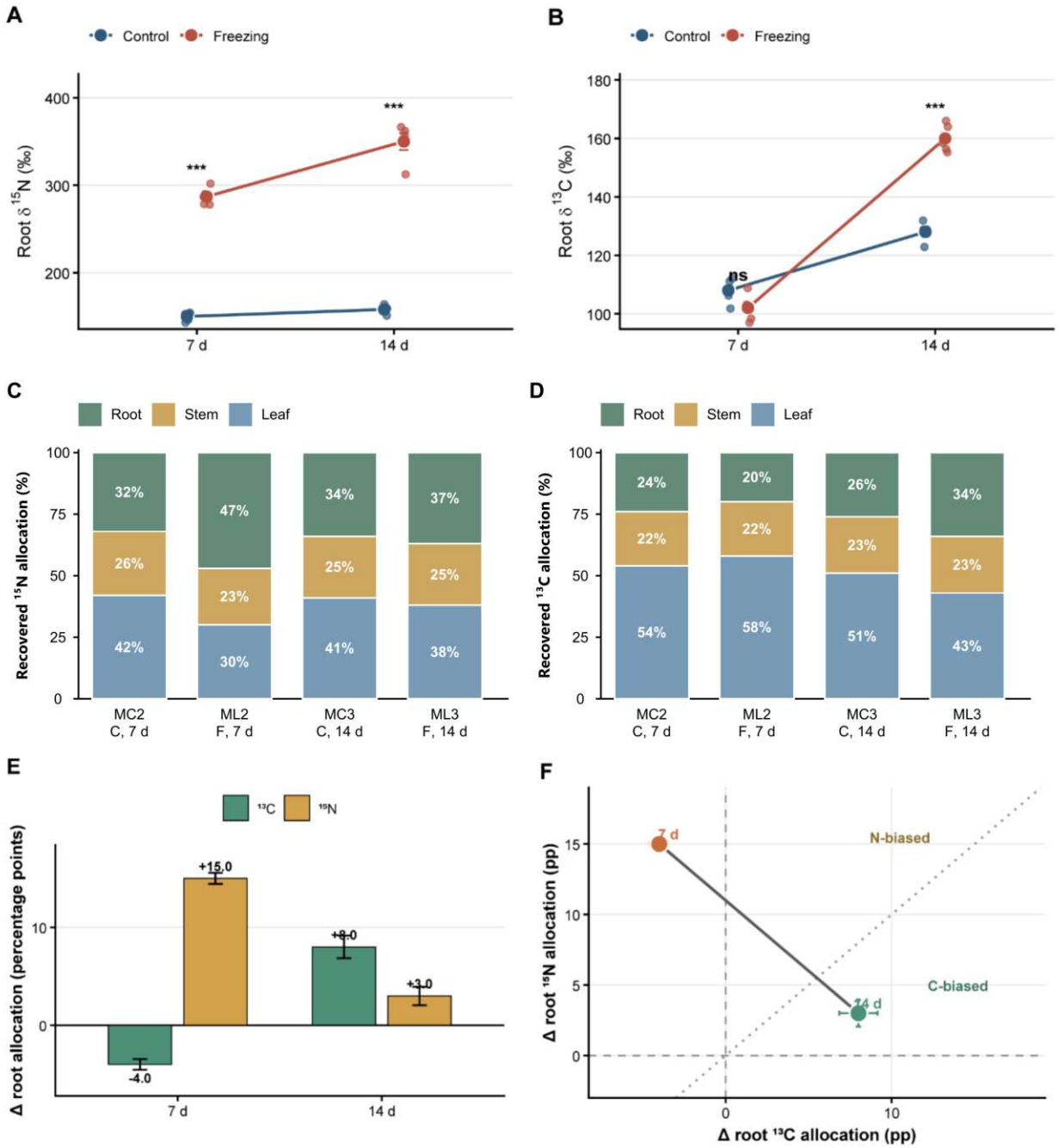

Fig. 3. Dual-isotope partitioning in plants exposed to different freezing durations.

(A) Root $\delta^{15}N$ values in control and freezing-treated plants sampled at 7 and 14 d. (B) Root $\delta^{13}C$ values in control and freezing-treated plants sampled at 7 and 14 d. (C) Proportional allocation of ^{15}N among roots, stems and leaves under control and freezing conditions at 7 and 14 d. (D) Proportional allocation of ^{13}C among roots, stems and leaves under control and freezing conditions at 7 and 14 d. (E) Freezing-induced changes in root ^{13}C and ^{15}N allocation at 7 and 14 d, expressed as percentage-point differences between freezing and the corresponding control. (F) Bivariate plot of freezing-induced changes in root ^{13}C and ^{15}N allocation at 7 and 14 d. The x-axis represents the change in root ^{13}C allocation and the y-axis represents the change in root ^{15}N allocation. For isotope analyses, n = 6 independent biological replicates per treatment × time point. Isotopic composition is expressed in delta notation (‰). Organ allocation was calculated as the proportion of recovered ^{13}C or ^{15}N present in roots, stems and leaves relative to total plant isotope recovery. Changes in root allocation were calculated as freezing allocation (%) − corresponding control allocation (%) and are expressed in percentage points (pp). Control and freezing treatments were compared using two-tailed Student's t-test. Bars represent means ± SE. Asterisks indicate significant differences between treatments:

***P < 0.001; ns, not significant. $\delta^{13}C$, carbon stable-isotope composition; $\delta^{15}N$, nitrogen stable-isotope composition; pp, percentage points.

Transcriptomic profiles identify nitrogen-associated and carbohydrate-associated responses

RNA-seq analysis revealed extensive transcriptional responses that differed between the two sampling times during freezing (Fig. 4). Principal component analysis clearly separated control and freezing-treated samples and further distinguished the 7- and 14-d responses, with PC1 and PC2 explaining 49.44% and 23.28% of the total variation, respectively (Fig. 4A). The number of detected DEGs increased with stress duration: 2,162 DEGs were identified at 7 d and 3,143 at 14 d (Fig. 4B). Only 824 DEGs were shared between the two stages, while 1,338 and 2,319 genes were specific to 7 and 14 d, respectively, indicating that the sets of genes meeting the DEG threshold differed substantially between the two sampling stages (Fig. 4C). KEGG enrichment analysis showed that 7-d DEGs were preferentially associated with nitrogen metabolism, alanine/aspartate/glutamate metabolism, arginine and proline metabolism, glutathione metabolism, peroxisome function and stress-signaling pathways, whereas 14-d DEGs were more strongly enriched in starch and sucrose metabolism, galactose metabolism, glycolysis/gluconeogenesis, carbon metabolism and ascorbate-related pathways (Fig. 4D). Consistent with this functional shift, genes involved in nitrogen and amino-acid adjustment, including GS1.1, GOGAT1, ASN1, P5CS1 and P4H1, showed strong freezing-responsive expression at 7 d, whereas genes associated with starch/sucrose turnover and compatible-solute metabolism, including AMY3, BAM3, SUS6, TPS1, TPP1, TRE1, GOLS1 and RS5, became particularly prominent at 14 d; cold/redox-related genes such as CBF3, COR47, APX2 and POD42 remained activated across the freezing period (Fig. 4E). Module-level scoring summarized these temporal patterns, showing that nitrogen/amino-acid adjustment was already strongly activated at 7 d, while starch/sucrose turnover and trehalose/RFO metabolism displayed their strongest induction at 14 d (Fig. 4F). Finally, qRT-PCR measurements closely agreed with RNA-seq estimates across representative genes ($R^2 = 0.872$), supporting agreement between the two expression assays (Fig. 4G). Thus, the transcriptional patterns paralleled the temporal differences observed in physiology and isotope allocation, with stronger nitrogen/amino-acid-related responses at 7 d and stronger carbohydrate-related responses at 14 d.

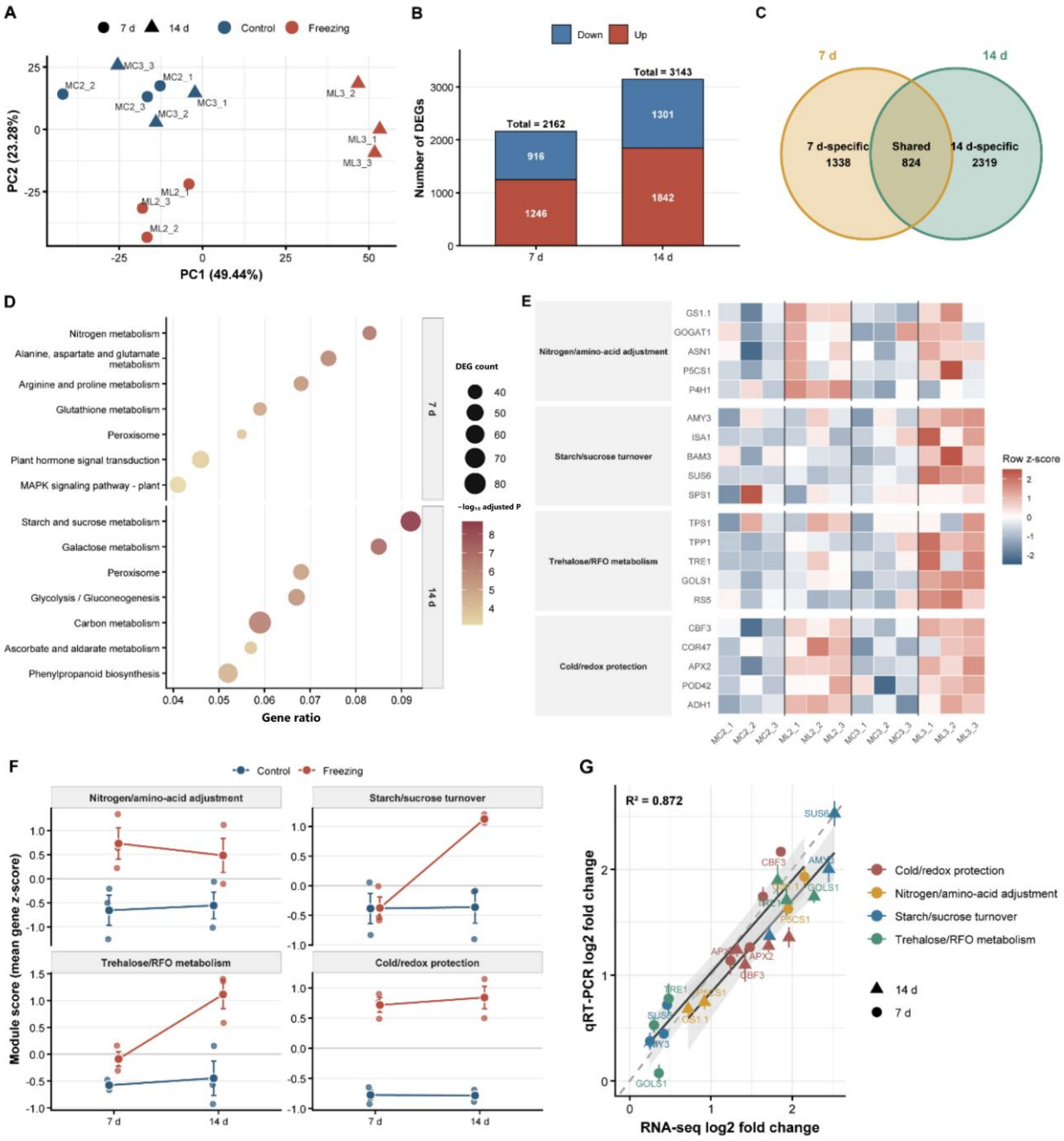

Fig. 4. Root transcriptomic responses to freezing at 7 and 14 days.

(A) Principal component analysis of RNA-seq profiles from control and freezing-treated roots sampled at 7 and 14 d. Each point represents one biological replicate. (B) Numbers of upregulated and downregulated differentially expressed genes in freezing-treated roots relative to the corresponding controls at 7 and 14 d. (C) Numbers of DEGs specific to the 7-d comparison, shared between the two time points, and specific to the 14-d comparison. (D) KEGG pathway enrichment analysis of DEGs identified at 7 and 14 d. Point size represents DEG count, the x-axis represents gene ratio, and color represents $-\log_{10}$(BH-adjusted P). (E) Heatmap of representative freezing-responsive genes assigned to nitrogen/amino-acid adjustment, starch/sucrose turnover, trehalose/RFO metabolism and cold/redox protection modules. Expression values were standardized by gene and are presented as row z-scores. (F) Module scores for nitrogen/amino-acid adjustment, starch/sucrose turnover, trehalose/RFO metabolism and cold/redox protection at 7 and 14 d. Module scores were calculated as the mean z-score of genes assigned to each functional module. (G) qRT-PCR validation of selected freezing-responsive genes. qRT-PCR-derived $\log_2$ fold changes are plotted

against RNA-seq-derived $\log_2$ fold changes; the coefficient of determination is shown in the panel. RNA-seq analysis included n = 3 independent biological replicates per treatment × time point, corresponding to MC2, ML2, MC3 and ML3 sample groups. DEGs were defined as FDR < 0.05 and $|\log_2$ fold change$| > 1$. KEGG enrichment was performed using the hypergeometric test, with multiple-testing correction based on BH-adjusted P value. qRT-PCR validation included n = 6 biological replicates and 3 technical replicates. Different lowercase letters, where shown, indicate significant differences at $P < 0.05$. DEG, differentially expressed gene; KEGG, Kyoto Encyclopedia of Genes and Genomes; RFO, raffinose-family oligosaccharide; qRT-PCR, quantitative reverse-transcription PCR; MC2, 7-d control; ML2, 7-d freezing; MC3, 14-d control; ML3, 14-d freezing.

Metabolomic profiles identify greater carbohydrate accumulation in the 14-day group

Metabolomic profiling further supported a temporally structured freezing response and identified differences in root metabolite profiles between 7 and 14 d (Fig. 5). Principal component analysis clearly separated freezing-treated samples from their corresponding controls and also distinguished the two treatment durations, indicating substantial stage-dependent metabolic remodeling (Fig. 5A). A total of 44 differentially accumulated metabolites (DAMs; 29 increased and 15 decreased) were detected at 7 d, compared with 43 DAMs (31 increased and 12 decreased) at 14 d, showing that the major distinction between the two stages lay in metabolite identity and pathway composition rather than the total number of altered metabolites (Fig. 5B). At 7 d, DAMs were preferentially enriched in alanine/aspartate/glutamate metabolism, arginine and proline metabolism, glutathione metabolism, nitrogen metabolism and the TCA cycle, whereas the 14-d response was dominated by starch and sucrose metabolism, galactose metabolism, glycolysis/gluconeogenesis, carbon metabolism and ascorbate-related pathways (Fig. 5C). The metabolite heatmap similarly revealed strong early changes in nitrogenous compounds, including glutamine, glutamate, GABA, arginine, ornithine and proline, whereas prolonged freezing produced coordinated accumulation of maltose, glucose, glucose-6-phosphate, UDP-glucose, sucrose, trehalose-6-phosphate, trehalose, myo-inositol, galactinol and raffinose (Fig. 5D). Targeted comparisons further showed that D-trehalose changed little at 7 d but increased sharply at 14 d, while sucrose, galactinol and raffinose also accumulated strongly during the late stage. Notably, L-proline concentrations were lower under freezing at both 7 and 14 d, whereas trans-4-hydroxy-L-proline increased, indicating that freezing altered these related metabolite pools in opposite directions (Fig. 5E). Mapping these metabolites alongside candidate genes grouped GS1.1/GOGAT1-associated glutamine/glutamate metabolism and P5CS1-associated proline metabolism with nitrogen-related responses, whereas starch/sucrose turnover and trehalose/RFO metabolism were prominent in the 14-d carbohydrate-associated profile (Fig. 5F). Together, these data

indicate nitrogen- and amino-acid-associated changes at 7 d and greater carbohydrate accumulation at 14 d, trehalose also shows a very high level of involvement at 14 days. We therefore integrated isotope, transcriptomic, metabolomic and physiological datasets to determine how these coordinated responses were associated with freezing tolerance.

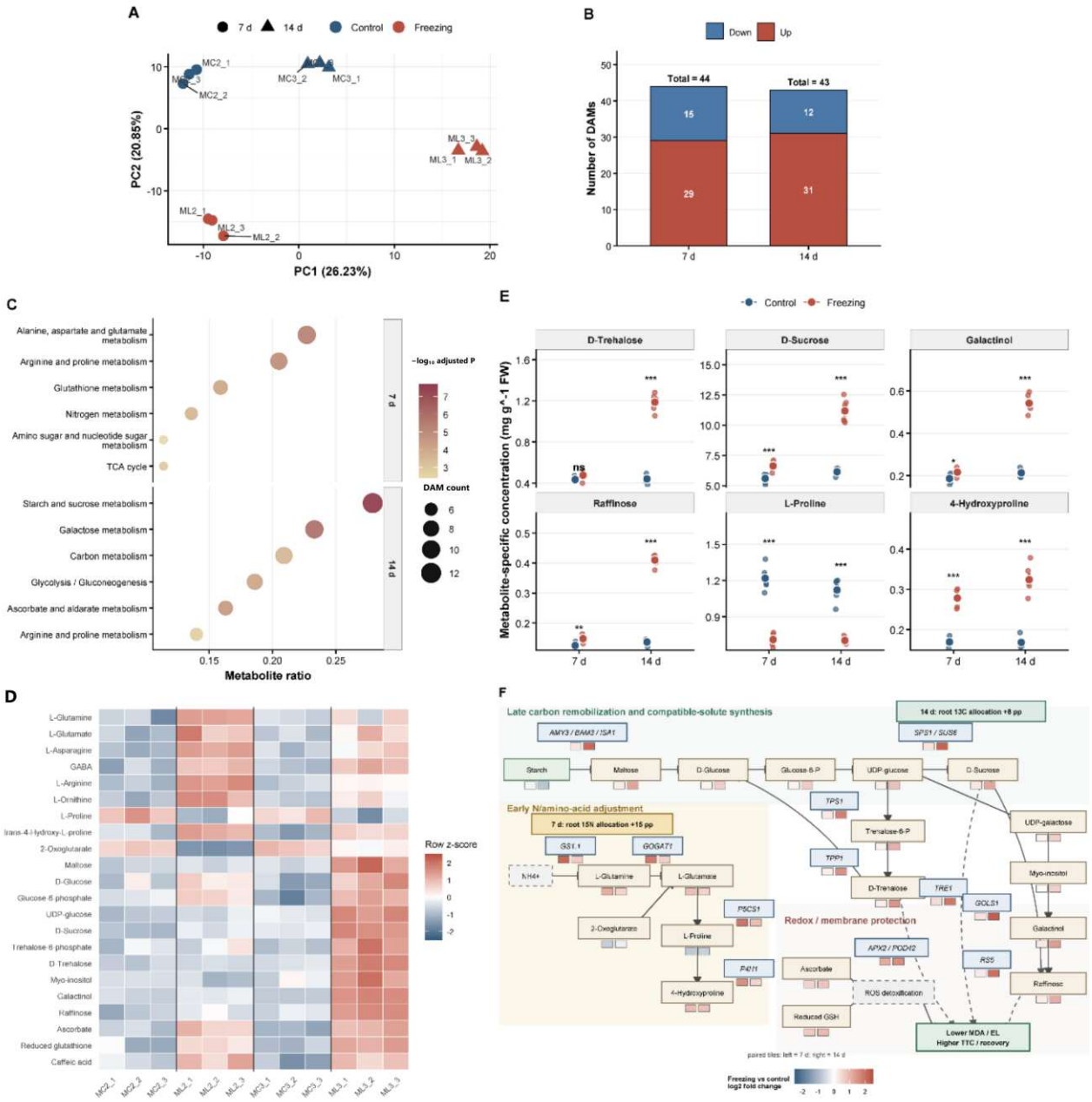

Fig. 5. Root metabolomic responses and carbon–nitrogen pathway mapping during freezing.

(A) Principal component analysis of root metabolite profiles from control and freezing-treated plants sampled at 7 and 14 d. Each point represents one biological replicate. (B) Numbers of increased and decreased differentially accumulated metabolites identified in freezing-treated roots relative to the corresponding controls at 7 and 14 d. (C) KEGG pathway enrichment analysis of DAMs at 7 and 14 d. Point size represents DAM count, the x-axis represents metabolite ratio, and color represents $-\log_{10}$(BH-adjusted P). (D) Heatmap of representative amino acids, organic acids, carbohydrates and antioxidant-related metabolites in control and freezing-treated roots at 7 and 14 d. Metabolite abundance was

standardized by metabolite and is presented as row z-scores. (E) Quantification of D-trehalose, D-sucrose, galactinol, raffinose, L-proline and trans-4-hydroxy-L-proline in control and freezing-treated roots at 7 and 14 d. (F) Schematic pathway map of nitrogen assimilation, amino-acid metabolism, starch degradation, sucrose metabolism, trehalose/RFO metabolism and redox-related metabolites. Paired tiles indicate freezing/control $\log_2$ fold changes at 7 d and 14 d, respectively. The map summarizes pathway annotations and abundance changes; it does not represent measured metabolic fluxes. Metabolomic profiling included n = 3 independent biological replicates per treatment × time point, corresponding to MC2, ML2, MC3 and ML3. KEGG pathway enrichment was performed using the hypergeometric test, with significance defined as BH-adjusted P value < 0.05. For panel E, bars represent means ± SE, and control and freezing treatments at each time point were compared using two-tailed Student's t-test. Asterisks indicate *P < 0.05, **P < 0.01, and ***P < 0.001; ns, not significant. DAM, differentially accumulated metabolite; RFO, raffinose-family oligosaccharide; GSH, glutathione; EL, electrolyte leakage; TTC, triphenyl tetrazolium chloride; pp, percentage points.

Multiblock integration links tracer partitioning, molecular profiles, and physiological traits

Integrated analysis of isotope, transcriptomic, metabolomic, and physiological datasets from matched biological replicates identified cross-layer covariation among the treatment–time groups (Fig. 6). Multi-omics ordination distinguished the treatment–time groups, with the first two integrated components explaining 56.93% and 28.94% of the total variation, respectively, indicating that the different molecular and physiological data layers shared a pronounced treatment- and time-associated multivariate structure (Fig. 6A). Pairwise RV coefficients further showed high cross-block similarity across the matched biological replicates, particularly between the metabolomic and physiological datasets (RV = 0.93) and between the physiological and isotope datasets (RV = 0.90), with substantial similarity also observed among the transcriptomic, metabolomic, and isotope data layers (Fig. 6B).

Balanced-subsample feature prioritization consistently identified galactinol, L-glutamine, maltose, SUS6, D-sucrose, L-glutamate, AMY3, root ^{15}N allocation, GOLS1, D-trehalose, root TTC activity, root ^{13}C allocation, MDA, GS1.1, ascorbate, and soluble sugar among the most frequently retained variables (Fig. 6C). Their repeated selection summarized a multivariate signature involving tracer partitioning, gene expression, metabolite abundance, and physiological status within this dataset.

The integrated heatmap showed that the 7-d freezing stage was characterized more strongly by root ^{15}N allocation and nitrogen-associated traits, whereas the 14-d freezing stage showed greater root ^{13}C allocation, higher expression of AMY3, SUS6, TPS1, and GOLS1, and greater accumulation of sucrose, trehalose, galactinol, raffinose, and soluble sugars. These late-stage changes coincided with lower MDA and electrolyte leakage and higher root TTC and antioxidant activities relative to the 7-d stage (Fig. 6D).

Cross-omics association analysis further identified relationships between root ^{15}N allocation, nitrogen-assimilation genes, and glutamine-related metabolism, whereas root ^{13}C allocation was associated with carbohydrate-turnover genes, protective sugars, and physiological indicators of membrane integrity and root activity (Fig. 6E). Consistently, the early N-adjustment module showed its strongest associations with nitrogen-related traits, whereas the late carbohydrate-protection module was positively associated with root ^{13}C allocation, soluble sugars, sucrose synthase, root TTC activity, and antioxidant capacity, and negatively associated with starch, electrolyte leakage, and MDA (Fig. 6F). Collectively, these associations distinguished a 7-d nitrogen-associated state from a 14-d carbohydrate-rich state with lower measured injury. Trehalose was prioritized as a candidate metabolite associated with the lower-injury state, and we next examined whether trehalose supplementation and trehalase inhibition altered freezing-related injury and recovery.

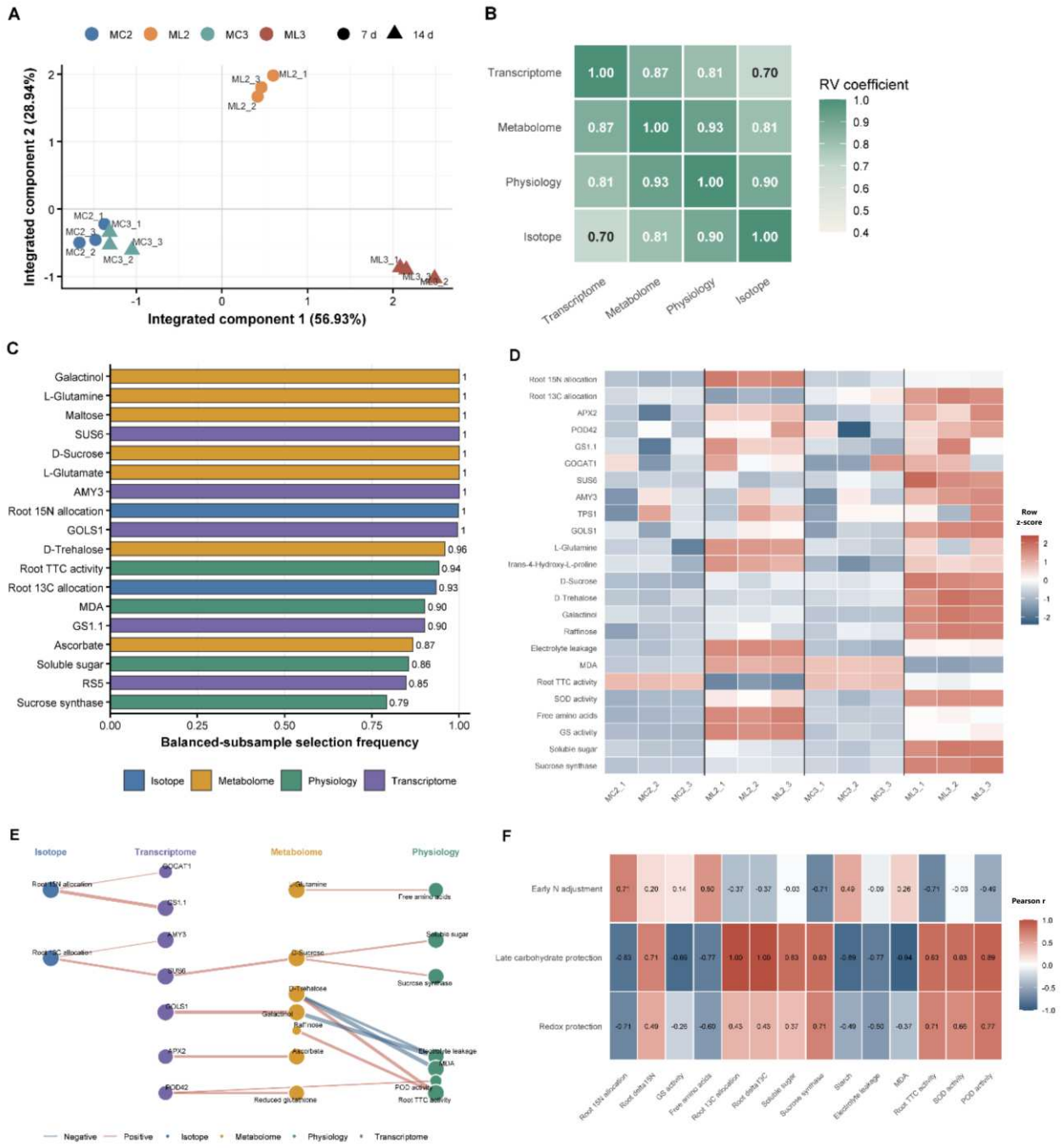

Fig. 6. Integration of isotope, transcriptomic, metabolomic, and physiological datasets.

(A) Integrated multivariate ordination of stable-isotope, transcriptomic, metabolomic and physiological data from control and freezing-treated plants at 7 and 14 d. Each point represents one biological replicate; percentages indicate variance explained by integrated components 1 and 2. (B) Pairwise RV coefficients among transcriptomic, metabolomic, physiological and stable-isotope datasets. Cell values indicate the RV coefficient for each pair of data blocks. (C) Balanced-subsample selection frequencies of variables retained across the integrated analysis. Variables are grouped by stable-isotope, metabolomic, physiological and transcriptomic data types. (D) Integrated heatmap of selected stable-isotope allocation variables, genes, metabolites and physiological traits across individual samples. Values were standardized within each variable and are displayed as z-scores. (E) Cross-omics association network linking stable-isotope, transcriptomic, metabolomic and physiological variables. Node categories indicate data type, and edge classes indicate positive or negative associations according to the threshold specified in the Methods. (F) Correlation matrix between integrated functional modules and selected isotope-allocation and

physiological traits. Cell values represent correlation coefficients. The integrated dataset comprised the 7-d control, 7-d freezing, 14-d control and 14-d freezing groups, with n = 3 biological replicates per group for the omics sample matrix. Preprocessing was specific to each data type, as described in Methods. Balanced resampling was repeated 1,000 times, and variables were ranked by selection frequency. Network edges were retained at $|r| \geq 0.6$ and adjusted $P < 0.01$, using Pearson correlations. Module–trait associations in panel F were calculated using Pearson correlation and corrected for multiple testing using the Benjamini–Hochberg (BH) procedure. RV, Robert–Escoufier RV coefficient; MDA, malondialdehyde; TTC, triphenyl tetrazolium chloride; GS, glutamine synthetase; RFO, raffinose-family oligosaccharide.

Pharmacological treatments support trehalose-associated protection during freezing

Pharmacological manipulation of trehalose metabolism was associated with improved root protection during freezing (Fig. 7). Exogenous trehalose increased root trehalose and trehalose-6-phosphate contents. Validamycin A reduced trehalase activity and increased trehalose retention, while the combined validamycin A and trehalose treatment produced the greatest trehalose accumulation among the freezing treatments (Fig. 7A).

Trehalose supplementation reduced freezing-induced electrolyte leakage and MDA accumulation, whereas mannitol, sorbitol, and sucrose generally produced weaker effects. The combined validamycin A and trehalose treatment showed particularly low membrane injury (Fig. 7B). These changes were accompanied by higher root TTC activity and increased SOD and POD activities, with the combined treatment producing among the strongest improvements in root metabolic and antioxidant status (Fig. 7C). Trehalose also improved survival and shoot and root regrowth after freezing. The tested alternative sugar and polyol treatments had more limited effects, whereas validamycin A plus trehalose produced among the strongest recovery responses (Fig. 7D). Comparisons among freezing, trehalose, validamycin A, and combined treatments showed that higher trehalose content coincided with lower electrolyte leakage and greater root TTC activity (Fig. 7E).

Expression profiling over 0–24 h showed treatment-associated responses in genes involved in trehalose metabolism, carbohydrate turnover, and cold/redox protection, including *MrTPS1*, *MrTPP1*, *MrTRE1*, *MrSUS6*, *MrAMY3*, *MrGOLS1*, *MrCBF3*, *MrCOR47*, and *MrAPX2*. Trehalose- and validamycin A-containing treatments generally enhanced these transcriptional responses (Fig. 7F). Together, the pharmacological results support trehalose-associated freezing protection and provide intervention-based evidence for the relevance of a carbohydrate pathway prioritized by the molecular profiles.

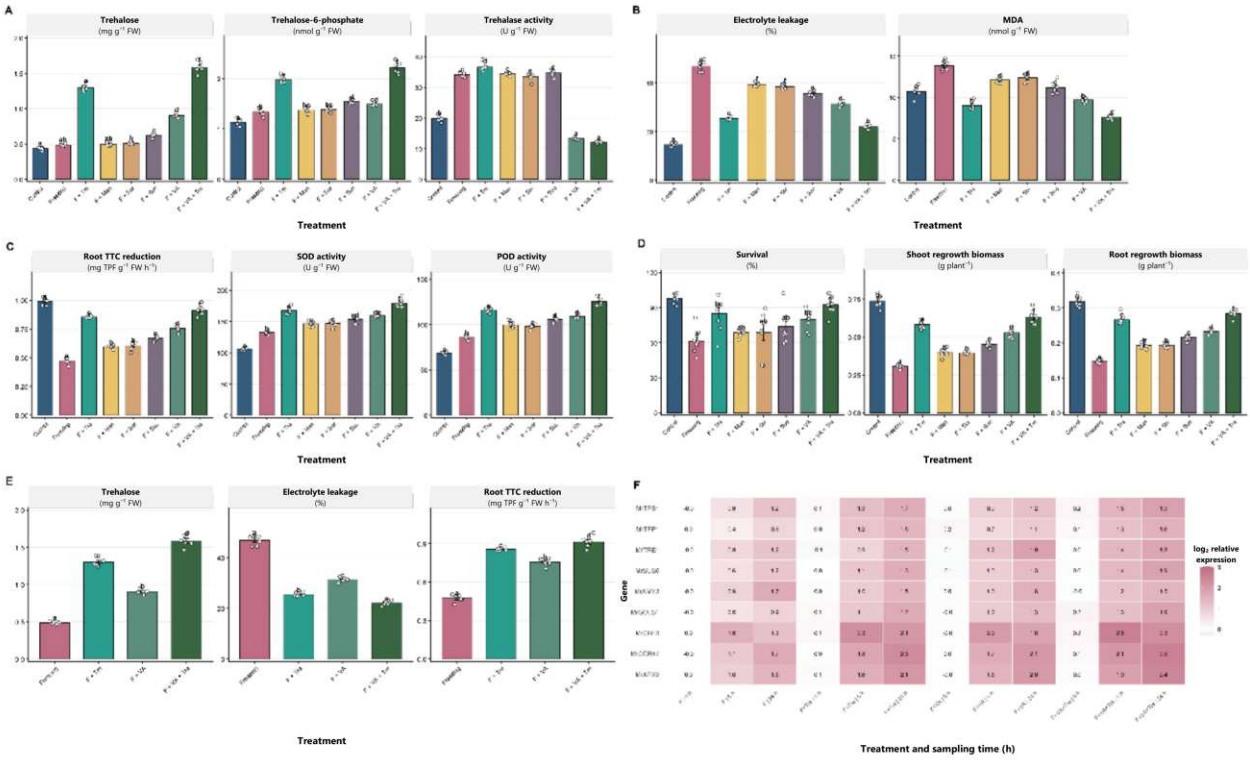

Fig. 7. Pharmacological manipulation of trehalose metabolism and freezing-related responses.

(A) Root trehalose content, trehalose-6-phosphate content and trehalase activity under Control, Freezing, F + Tre, F + Man, F + Sor, F + Suc, F + VA and F + VA + Tre treatments. (B) Root electrolyte leakage and MDA content under the eight treatments. (C) Root TTC activity, SOD activity and POD activity under the eight treatments. (D) Survival rate and shoot and root regrowth after freezing and recovery under the eight treatments. (E) Trehalose content, electrolyte leakage and root TTC activity in Freezing, F + Tre, F + VA and F + VA + Tre treatments. (F) Gene expression at 0, 6, and 24 h under Freezing, F + Tre, F + VA, and F + VA + Tre treatments, shown as $\log_2$ relative expression. Facet headings specify endpoint units. Panels A–E comprise n = 6 biological replicates per treatment; expression measurements comprise n = 6 biological replicates with three technical replicates per treatment × time point. Survival was analyzed as a binomial response. Bars represent means ± SE. Different lowercase letters indicate differences among treatments at $P < 0.05$. Tre, trehalose; Man, mannitol; Sor, sorbitol; Suc, sucrose; VA, validamycin A; T6P, trehalose-6-phosphate; EL, electrolyte leakage; MDA, malondialdehyde; TTC, triphenyl tetrazolium chloride; SOD, superoxide dismutase; POD, peroxidase; F, freezing.

Discussion

Contrasting root metabolic states accompany differences in injury and recovery

The 7-d and 14-d groups exhibited contrasting root metabolic and injury states. The concurrent decline in starch and increase in soluble sugars and sucrose synthase activity at 14 d were consistent with carbohydrate remodeling. Such changes agree with the established importance of compatible solutes during cold responses and with the temperature sensitivity of starch and sucrose metabolism [1,15,16].

Free amino acids and glutamine synthetase activity peaked at 7 d, together with stronger nitrogen-related molecular responses. Amino acids can contribute to nitrogen redistribution, metabolic buffering, and osmotic adjustment, while glutamine synthetase is central to nitrogen assimilation [17,18]. These traits indicate a stronger nitrogen-associated response at 7 d but do not establish that this response reduced injury. MDA and electrolyte leakage were also greatest at this sampling stage.

Lower injury and higher root TTC activity at 14 d were accompanied by better post-freezing survival and regrowth. These endpoints describe complementary aspects of freezing performance [2]. Changes in membrane integrity, antioxidant defense, and cold-responsive gene expression provide plausible physiological context [19–21]. However, the present −10 °C exposure is distinct from classical acclimation at non-freezing temperatures [1]. Independent destructive samples, differences in surviving tissues, and the timing of thawing and recovery limit any inference that the same individuals recovered during continued freezing. The observations therefore support different response states rather than a demonstrated continuous adaptive trajectory.

Relative tracer partitioning provides an organ-level context for root metabolism

The freezing-induced increase in the root share of recovered ^{15}N was greater at 7 d than at 14 d, whereas the root share of recovered ^{13}C increased at 14 d. Carbon and nitrogen allocation can respond to temperature, nutrient availability, and changing organ demands [22–24]. Here, the approximately 15-percentage-point increase in root ^{15}N allocation at 7 d coincided with increased free amino acids and GS activity, while the approximately 8-percentage-point increase in root ^{13}C allocation at 14 d coincided with greater carbohydrate accumulation.

Together, the isotope and physiological profiles suggest stage-dependent coordination between relative tracer allocation to roots and carbon–nitrogen metabolic adjustment during freezing. The stronger root ^{15}N allocation response at 7 d aligns with enhanced amino acid metabolism, whereas the more pronounced root ^{13}C allocation response at 14 d accompanies carbohydrate accumulation, suggesting distinct metabolic adjustments as freezing progresses.

Molecular profiles identify carbohydrate metabolism as a candidate protective response

The transcriptome and metabolome revealed both common and time-dependent responses to freezing. Cold-responsive transcription involves multiple regulatory pathways beyond the canonical CBF pathway

[25], and studies of alfalfa and other species have documented extensive changes in amino-acid, carbohydrate, and antioxidant metabolism during low-temperature exposure [4,5,26,27]. The partly distinct DEG sets at 7 and 14 d describe differences in threshold-defined responses; a gene detected as differential at only one time does not necessarily show a significant treatment × time interaction.

The nitrogen-associated profile at 7 d and carbohydrate-rich profile at 14 d were consistent across molecular and physiological measurements. Previous transcript–metabolite studies have similarly shown broad but non-identical changes across expression and metabolite pools during cold responses [28–34]. The late accumulation of trehalose, sucrose, galactinol, and raffinose is compatible with proposed protective roles of soluble sugars. Galactinol and raffinose can contribute to redox protection, and galactinol synthesis has been linked to cold responses in cucumber and petunia [35–37].

Concurrent induction of TPS1, TPP1, and TRE1 suggests coordinated regulation of trehalose biosynthesis and turnover during freezing. Upregulation of a proline biosynthesis-associated gene, together with decreased free proline and increased hydroxyproline, further indicates remodeling of amino-acid metabolism. Collectively, these transcriptional and metabolic patterns are consistent with an integrated carbon–nitrogen response involving adjustments in trehalose metabolism and amino-acid pools during freezing.

Multiblock integration prioritizes candidates

Integration placed relative isotope partitioning alongside molecular profiles and physiological injury. The 7-d state aligned more strongly with root ^{15}N allocation and nitrogen-associated variables, whereas the 14-d state aligned with root ^{13}C allocation, carbohydrate-turnover genes, soluble sugars, and lower injury. Related concordance among molecular and physiological layers has been reported in low-temperature studies of alfalfa and other plants [30,34,38].

Nevertheless, all data blocks shared treatment and time effects. With three matched biological replicates per group, high RV coefficients and repeated feature selection may partly reflect group separation. Resampling does not add independent biological replication, and cross-block correlations do not establish direct regulatory relationships. Trehalose was prioritized because it appeared across several associated layers; its protective relevance was then examined using pharmacological treatments rather than inferred as a causal relationship from the network alone.

Pharmacological evidence for trehalose-associated freezing protection

The pharmacological experiments extend the observational profiles by showing that trehalose supplementation and trehalase inhibition altered measured freezing-related traits. Trehalose metabolism links carbon status and stress responses, and T6P is involved in the regulation of carbon use and source–sink relations [7,39]. Exogenous trehalose reduced electrolyte leakage and MDA and improved root TTC activity, antioxidant activities, survival, and regrowth. These effects are consistent with the wider literature linking trehalose-related metabolism to low-temperature responses, including *ScAREB4*-associated freezing tolerance in potato, *AtTPPI*-associated chilling tolerance in Arabidopsis, and *TaTPS11*-associated cold resistance in wheat [40–42].

The tested equimolar mannitol, sorbitol, and sucrose treatments generally provided weaker protection than trehalose. This comparison suggests that the observed responses were not fully reproduced by those controls under the tested conditions. It does not establish equal uptake, intracellular concentration, or metabolic effects, and cannot uniquely separate osmotic protection from signaling or carbon-metabolic responses. Trehalose treatment has also been associated with antioxidant regulatory responses in oriental melon [43], consistent with the changes in SOD and POD activities observed here.

Validamycin A treatment reduced trehalase activity while increasing trehalose content in the same root tissue, providing evidence that the intended metabolic response occurred. This is important because validamycin A responses can be tissue dependent [14].

Collectively, these findings support trehalose-associated protection as part of a broader carbohydrate response involving galactinol and raffinose [35,44]. The supplementation and inhibition experiments link changes in trehalose availability and turnover with root responses to freezing, while the protective effects of exogenous trehalose encompass membrane integrity, antioxidant defense, and root vitality. These physiological benefits extend to survival and regrowth after freezing, highlighting trehalose metabolism as an important component of root freezing resilience.

Conclusions

Medicago ruthenica roots showed distinct metabolic and injury states at 7 and 14 d of freezing. Stronger nitrogen- and amino-acid-associated responses and a larger increase in the root share of recovered ^{15}N characterized the 7-d group. Greater relative root ^{13}C partitioning, carbohydrate accumulation, lower

injury, and better post-freezing recovery characterized the 14-d group. Multiomics integration linked starch–sucrose turnover and trehalose/RFO metabolism to this carbohydrate-rich state. Exogenous trehalose and validamycin A treatments support trehalose-associated freezing protection through changes in membrane injury, root metabolic activity, antioxidant responses, and recovery. Together, these findings highlight stage-dependent carbon–nitrogen metabolic adjustment and trehalose-associated protection as important features of root freezing resilience in *M. ruthenica*.

Abbreviations

BH, Benjamini–Hochberg; DAM, differentially accumulated metabolite; DEG, differentially expressed gene; EL, electrolyte leakage; EL50, temperature at 50% electrolyte leakage; FW, fresh weight; GS, glutamine synthetase; MDA, malondialdehyde; PCA, principal component analysis; POD, peroxidase; pp, percentage points; qRT-PCR, quantitative reverse-transcription PCR; RFO, raffinose-family oligosaccharide; RV, Robert–Escoufier coefficient; SOD, superoxide dismutase; SS-I, sucrose synthase assayed in the cleavage direction; T6P, trehalose-6-phosphate; TPF, triphenyl formazan; TTC, triphenyl tetrazolium chloride; VA, validamycin A.

Declarations

Ethics approval and consent to participate

Not applicable.

Consent for publication

Permission has been obtained to collect *Medicago ruthenica* L. cv. ' Zhilixing '.

Availability of data and materials

The datasets used and analyzed during the current study are available from the corresponding author on reasonable request.

Competing interests

The authors declare that they have no competing interests.

Data availability

The datasets generated and/or analysed during the current study are available in the NCBI repository, PRJNA1558789.

Funding

Science and Technology Support Project for "Double First-Class" Development in the Inner Mongolia Autonomous Region (contract no. 2026SYLZLZJ005); 2026 Open Research Fund of the Institute of Water Resources for Pastoral Areas, Ministry of Water Resources: Research on the Adaptive Strategies and Regulatory Mechanisms of Functional Traits in *Medicago ruthenica* under Combined Cold and Drought Stress in the Desert Steppe North of the Yinshan Mountains (contract no. YSS202604).

Authors' contributions

JX: methodology, and methodology and writing—original draft. YM: conceptualization, formal analysis and data curation. YZ and JW: project administration and investigation. KC: writing—review and editing. WF: investigation and formal analysis. FS: resources.

References

1. Thomashow MF. PLANT COLD ACCLIMATION: Freezing Tolerance Genes and Regulatory Mechanisms. Annual Review of Plant Physiology and Plant Molecular Biology. 1999;50:571-599. https://doi.org/10.1146/annurev.arplant.50.1.571.

2. Verslues PE, Agarwal M, Katiyar-Agarwal S, Zhu J, Zhu JK. Methods and concepts in quantifying resistance to drought, salt and freezing, abiotic stresses that affect plant water status. The Plant Journal. 2006;45:523-539. https://doi.org/10.1111/j.1365-313X.2005.02593.x.

3. Wang T, Ren L, Li C, Zhang D, Zhang X, Zhou G, et al. The genome of a wild Medicago species provides insights into the tolerant mechanisms of legume forage to environmental stress. BMC Biology. 2021;19:96. https://doi.org/10.1186/s12915-021-01033-0.

4. Wang X, Kang W, Wu F, Miao J, Shi S. Comparative Transcriptome Analysis Reveals New Insight of Alfalfa (*Medicago sativa* L.) Cultivars in Response to Abrupt Freezing Stress. Frontiers in Plant Science. 2022;13:798118. https://doi.org/10.3389/fpls.2022.798118.

627 5. Pu X, Fu Y, Xu C, Li X, Wang W, De K, et al. Transcriptomic analyses provide molecular insight into
628 the cold stress response of cold-tolerant alfalfa. BMC Plant Biology. 2024;24:741.
629 https://doi.org/10.1186/s12870-024-05136-y.

630 6. Xu P, Ma W, Feng H, Cai W. The NAC056 transcription factor confers freezing tolerance by positively
631 regulating expression of CBFs and NIA1 in Arabidopsis. Plant Communications. 2024;5:100923.
632 https://doi.org/10.1016/j.xplc.2024.100923.

633 7. Paul MJ, Primavesi LF, Jhurreea D, Zhang Y. Trehalose Metabolism and Signaling. Annual Review of
634 Plant Biology. 2008;59:417-441. https://doi.org/10.1146/annurev.arplant.59.032607.092945.

635 8. Li HW, Zang BS, Deng XW, Wang XP. Overexpression of the trehalose-6-phosphate synthase gene
636 *OsTPS1* enhances abiotic stress tolerance in rice. Planta. 2011;234:1007-1018.
637 https://doi.org/10.1007/s00425-011-1458-0.

638 9. Shu Y, Zhang W, Tang L, Li Z, Liu X, Liu X, et al. ABF1 Positively Regulates Rice Chilling Tolerance
639 via Inducing Trehalose Biosynthesis. International Journal of Molecular Sciences. 2023;24:11082.
640 https://doi.org/10.3390/ijms241311082.

641 10. Liu G, Qin H, Wang Y, Wang Y, Xu P, Zhao Y, et al. *VaTPS9* from *Vitis amurensis* Encodes a
642 Trehalose-6-Phosphate Synthase Correlated with Cold Tolerance. Plants. 2026;15:847.
643 https://doi.org/10.3390/plants15050847.

644 11. SHIMOSAKA E, OZAWA K. Overexpression of cold-inducible wheat galactinol synthase confers
645 tolerance to chilling stress in transgenic rice. Breeding Science, 2015, 65(5): 363-371.
646 https://doi.org/10.1270/jsbbs.65.363.

647 12. Zuther E, Büchel K, Hundertmark M, Stitt M, Hincha DK, Heyer AG. The role of raffinose in the cold
648 acclimation response of *Arabidopsis thaliana*. FEBS Letters. 2004;576:169-173.
649 https://doi.org/10.1016/j.febslet.2004.09.006.

650 13. Pennycooke JC, Jones ML, Stushnoff C. Down-Regulating α-Galactosidase Enhances Freezing
651 Tolerance in Transgenic Petunia. Plant Physiology. 2003;133:901-909.
652 https://doi.org/10.1104/pp.103.024554.

14. López M, Tejera NA, Lluch C. Validamycin A improves the response of *Medicago truncatula* plants to salt stress by inducing trehalose accumulation in the root nodules. Journal of Plant Physiology. 2009;166:1218-1222. https://doi.org/10.1016/j.jplph.2008.12.011.

15. Koster KL, Lynch DV. Solute Accumulation and Compartmentation during the Cold Acclimation of Puma Rye. Plant Physiology. 1992;98:108-113. https://doi.org/10.1104/pp.98.1.108.

16. Seydel C, Kitashova A, Fürtauer L, Nägele T. Temperature-induced dynamics of plant carbohydrate metabolism. Physiologia Plantarum. 2022;174:e13602. https://doi.org/10.1111/ppl.13602.

17. Singh K, Gulyás Z, Athmer B, Kovács B, Mednyánszky Z, Galiba G, et al. Comparative study of free amino acids at metabolite and gene expression levels in Triticeae during cold acclimation. Journal of Plant Biochemistry and Biotechnology. 2024;33:558-569. https://doi.org/10.1007/s13562-024-00912-1.

18. Yin H, Yang F, He X, Du X, Mu P, Ma W. Advances in the functional study of glutamine synthetase in plant abiotic stress tolerance response. The Crop Journal. 2022;10:917-923. https://doi.org/10.1016/j.cj.2022.01.003.

19. Wang Y, Wang J, Sarwar R, Zhang W, Geng R, Zhu KM, et al. Research progress on the physiological response and molecular mechanism of cold response in plants. Frontiers in Plant Science. 2024;15:1334913. https://doi.org/10.3389/fpls.2024.1334913.

20. Guy CL. Cold Acclimation and Freezing Stress Tolerance: Role of Protein Metabolism. Annual Review of Plant Physiology and Plant Molecular Biology. 1990;41:187-223. https://doi.org/10.1146/annurev.pp.41.060190.001155.

21. Guo X, Liu D, Chong K. Cold signaling in plants: Insights into mechanisms and regulation. Journal of Integrative Plant Biology. 2018;60:745-756. https://doi.org/10.1111/jipb.12706.

22. Sun T, Ruan J, Cao T, Yao L, Zhao Z, Zhang J, et al. Effects of low-temperature stress during rice heading stage on carbon and nitrogen allocation in paddy eco-system of northeastern China. Frontiers in Plant Science. 2025;16:1484734. https://doi.org/10.3389/fpls.2025.1484734.

23. Zhou X, Ouyang S, Saurer M, Feng M, Bose AK, Duan H, et al. Species-specific responses of C and N allocation to N addition: evidence from dual 13C and 15N labeling in three tree species. Science of The Total Environment. 2024;927:172164. https://doi.org/10.1016/j.scitotenv.2024.172164.

680 24. POORTER H, NIKLAS K J, REICH P B, et al. Biomass allocation to leaves, stems and roots: meta-
681 analyses of interspecific variation and environmental control. New Phytologist, 2012, 193(1): 30–50.
682 https://doi.org/10.1111/j.1469-8137.2011.03952.x.

683 25. Fowler S, Thomashow MF. Arabidopsis Transcriptome Profiling Indicates That Multiple Regulatory
684 Pathways Are Activated during Cold Acclimation in Addition to the CBF Cold Response Pathway[W].
685 The Plant Cell. 2002;14:1675-1690. https://doi.org/10.1105/tpc.003483.

686 26. Xu H, Zhang Z, Zhao Q, Gao Y, Xiang Y, Chai J, et al. Study on molecular response of alfalfa to low
687 temperature stress based on transcriptomic analysis. BMC Plant Biology. 2024;24:1244.
688 https://doi.org/10.1186/s12870-024-05987-5.

689 27. He Y, Zhang Y, Li J, Ren Z, Zhang W, Zuo X, et al. Transcriptome dynamics in Artemisia annua
690 provides new insights into cold adaptation and de-adaptation. Frontiers in Plant Science. 2024;15:1412416.
691 https://doi.org/10.3389/fpls.2024.1412416.

692 28. Kaplan F, Kopka J, Sung DY, Zhao W, Popp M, Porat R, et al. Transcript and metabolite profiling
693 during cold acclimation of Arabidopsis reveals an intricate relationship of cold-regulated gene expression
694 with modifications in metabolite content. The Plant Journal. 2007;50:967-981.
695 https://doi.org/10.1111/j.1365-313X.2007.03100.x.

696 29. Song X, Wang H, Wang Y, Zeng Q, Zheng X. Metabolomics combined with physiology and
697 transcriptomics reveal how Nicotiana tabacum leaves respond to cold stress. Plant Physiology and
698 Biochemistry. 2024;208:108464. https://doi.org/10.1016/j.plaphy.2024.108464.

699 30. Wang Y, Sun Z, Wang Q, Xie J, Yu L. Transcriptomics and metabolomics revealed that phosphate
700 improves the cold tolerance of alfalfa. Frontiers in Plant Science. 2023;14:1100601.
701 https://doi.org/10.3389/fpls.2023.1100601.

702 31. MAO C, LI L, YANG T, et al. Transcriptomics integrated with widely targeted metabolomics reveals
703 the cold resistance mechanism in Hevea brasiliensis. Frontiers in Plant Science, 2023, 13: 1092411.
704 https://doi.org/10.3389/fpls.2022.1092411.

705 32. Yang X, Han Y, Huo G, Ge G, He S, Yang X, et al. Integrated transcriptomic and metabolomic
706 analysis provides insights into cold tolerance in lettuce (Lactuca sativa L.). BMC Plant Biology.
707 2024;24:442. https://doi.org/10.1186/s12870-024-05099-0.

33. Tang W, Li Z, Xu Z, Sui X, Liang L, Xiao J, et al. Transcriptomic and metabolomic analysis reveal the cold tolerance mechanism of common beans under cold stress. BMC Plant Biology. 2025;25:340. https://doi.org/10.1186/s12870-025-06333-z.

34. Fahim AM, Cao L, Li M, Gang Y, Rahman FU, Yuanyuan P, et al. Integrated transcriptome and metabolome analysis revealed hub genes and metabolites associated with subzero temperature tolerance following cold acclimation in rapeseed (Brassica rapa L.). Plant Physiology and Biochemistry. 2025;221:109647. https://doi.org/10.1016/j.plaphy.2025.109647.

35. Nishizawa A, Yabuta Y, Shigeoka S. Galactinol and Raffinose Constitute a Novel Function to Protect Plants from Oxidative Damage . Plant Physiology. 2008;147:1251-1263. https://doi.org/10.1104/pp.108.122465.

36. Dai H, Zhu Z, Wang Z, Zhang Z, Kong W, Miao M. Galactinol synthase 1 improves cucumber performance under cold stress by enhancing assimilate translocation. Horticulture Research. 2022;9:uhab063. https://doi.org/10.1093/hr/uhab063.

37. Zhang H, Sun Z, Feng S, Zhang J, Zhang F, Wang W, et al. The C2H2-type zinc finger protein PhZFP1 regulates cold stress tolerance by modulating galactinol synthesis in Petunia hybrida. Journal of Experimental Botany. 2022;73:6434-6448. https://doi.org/10.1093/jxb/erac274.

38. Ren N, Liu J, Wang H, Liu Z, Liu X, Li G. Combined transcriptomic and proteomic analysis reveals the response mechanisms of alfalfa to freezing stress. Frontiers in Plant Science. 2026;16:1682825. https://doi.org/10.3389/fpls.2025.1682825.

39. Raza A, Bhardwaj S, Atikur Rahman M, García-Caparrós P, Habib M, Saeed F, et al. Trehalose: A sugar molecule involved in temperature stress management in plants. The Crop Journal. 2024;12:1-16. https://doi.org/10.1016/j.cj.2023.09.010.

40. Liu T, Wang J, Chen L, Liu S, Liu T, Yu L, et al. *ScAREB4* promotes potato constitutive and acclimated freezing tolerance associated with enhancing trehalose synthesis and oxidative stress tolerance. Plant, Cell & Environment. 2023;46:3839-3857. https://doi.org/10.1111/pce.14707.

41. Lin Q, Wang J, Gong J, Zhang Z, Wang S, Sun J, et al. The *Arabidopsis thaliana* trehalose-6-phosphate phosphatase gene *AtTPPI* improve chilling tolerance through accumulating soluble sugar and

735 JA. Environmental and Experimental Botany. 2023;205:105117.
736 https://doi.org/10.1016/j.envexpbot.2022.105117.
737 42. Lu X, Zhang F, Zhang C, Li G, Du Y, Zhao C, et al. *TaTPS11* enhances wheat cold resistance by
738 regulating source-sink factor. Plant Physiology and Biochemistry. 2024;211:108695.
739 https://doi.org/10.1016/j.plaphy.2024.108695.
740 43. Xu D, Han Y, Zhang Y, Khan A, Dong L, Shao L, et al. CmTGA8-CmAPX1/CmGSTU25 regulatory
741 model involved in trehalose induced cold tolerance in oriental melon seedlings. Plant Physiology and
742 Biochemistry. 2025;220:109432. https://doi.org/10.1016/j.plaphy.2024.109432.
743 44. Shu P, Li Y, Sheng J, Shen L. Tomato SlMAPK3 Modulates Cold Resistance by Regulating the
744 Synthesis of Raffinose and the Expression of SlWRKY46. Journal of Agricultural and Food Chemistry.
745 2024;72:5185-5196. https://doi.org/10.1021/acs.jafc.3c09066.